

# Assessment of the performance of X-band satellite radar data for landslide mapping and monitoring: Upper Tena Valley case study

D. Notti<sup>1</sup>, J. C. Davalillo<sup>2</sup>, G. Herrera<sup>2</sup>, and O. Mora<sup>3</sup>

<sup>1</sup>Department of Earth Sciences, University of Pavia, Via Ferrata, 1, 27100 Pavia, Italy

<sup>2</sup>Área de Peligrosidad y Riesgos Geológicos, Departamento de Investigación y Prospectiva Geocientífica, Instituto Geológico y Minero de España (IGME), c/ Alenza 1, 28003 Madrid, Spain

<sup>3</sup>Altamira Information, c/ Còrsega, 381-387, 2n 3a, 08037 Barcelona, Spain

Received: 21 May 2010 – Revised: 22 July 2010 – Accepted: 2 August 2010 – Published: 7 September 2010

**Abstract.** The aim of this work is to analyse the advantages and disadvantages of using the new X-band SAR data acquired by TerraSAR-X sensors for landslides mapping. This dataset has been processed using a Persistent Scatterer Interferometry technique over the Upper Tena Valley (Central Pyrenees, Spain). In the first section, the geological and geomorphological setting of the study area is introduced, focusing on the description of the landslide inventory. Then the Stable Point Network technique is briefly described, followed by the assessment of the performance of the X-band SAR dataset. In this context, we present first a model to predict the distribution of Persistent Scatterers based on the slope geometry and the land use information, which has then been validated with X-band data results. On a second stage, we have assessed the performance of X-band dataset to detect and monitor mapped landslides. Finally some illustrative case studies are shown demonstrating the potential of using X-band SAR data not only for landslide mapping but also to detect and monitor deformations affecting human infrastructures.

## 1 Introduction

In the last decade satellite radar differential interferometry (DInSAR) has become a very useful remote-sensing tool for the detection and monitoring of active geological processes as landslides (Strozzi et al., 2010). The application of DInSAR to landslide research has been improved by the development of the Persistent Scatterers Interferometry techniques (PSI), as well as by the increasing availability of SAR data from different satellite sensors. The first

PSI method, namely the Permanent Scatterers technique (PSInSAR<sup>TM</sup>), was developed by Ferretti et al. (2001), which was followed by other authors that developed similar methods (Berardino et al., 2002; Mora et al., 2003; Arnaud et al., 2003; Pepe et al., 2005; Crosetto et al., 2005). Several interesting applications of these PSI techniques to landslide research can be found in Farina et al. (2006); Colesanti et al. (2006); Meisina et al. (2006, 2008, 2010); Pancioli et al. (2008); Wasowski et al. (2008); Herrera et al. (2009a, 2010); Cascini et al. (2009); Fernandez et al. (2009) and Righini et al. (2010). In the last 20 years, several different radar interferometry satellite missions have been launched providing different types of SAR images that can be used for ground movement detection and monitoring. C-Band satellites (ERS, ENVISAT or RADARSAT) operate at a 5.6 cm wavelength, covering wide areas at a low cost and providing data since the 1990s. They are good for the regional analysis of very slow landslides. L-Band satellite (ALOS PALSAR) operates at a 24 cm wavelength, permitting to detect faster landslides even in vegetated areas. Finally, the new X-band sensors (TerraSAR, Cosmo-Skymed) operate at 3 cm wavelength with the highest temporal and spatial sampling, allowing the detection and monitoring of movements affecting small areas with great detail.

In this context, the aim of this work is to assess the performance of the new X-band data from TerraSAR-X satellite for landslides mapping.

## 2 Introduction to the study area

The study area is the Upper Tena Valley, which is the upper part of the catchment area of River Gállego (Central Spanish Pyrenees). This area has an extension of 47 km<sup>2</sup> showing a WNW-ESE direction and a topographical gradient variation from 2500 to 1200 m a.s.l. (Fig. 1).



Correspondence to: J. C. Davalillo  
(jc.garcia@igme.es)

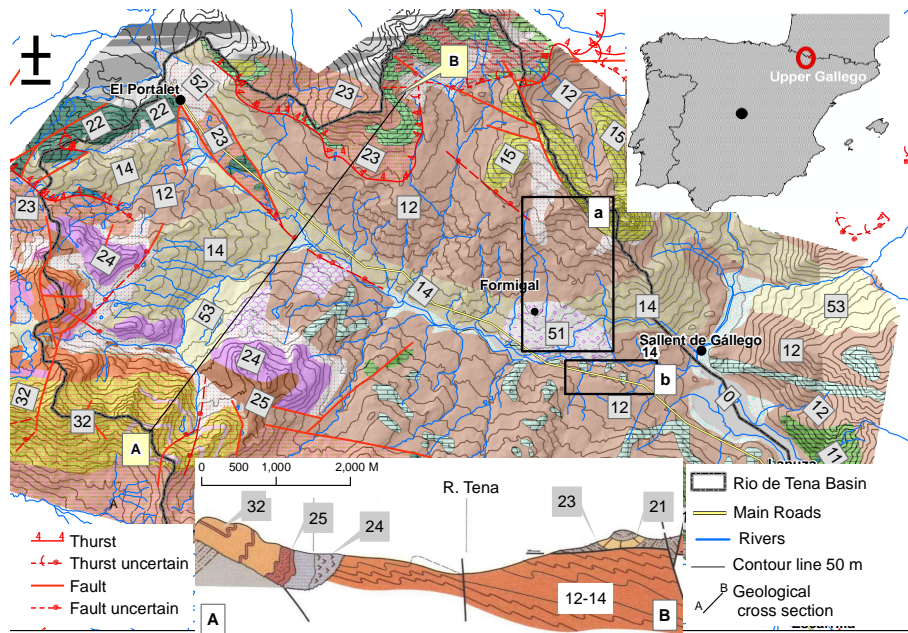


**Fig. 1.** Geology of the study area. 10: Limestone with shale, 11: Limestone “Dalle Formation”, 12: Shale, 13: Limestone vacuum, 14: Shale with sandstone, 15: Sandy Limestone “Foratata formation”, 20: Interbedded Shale-limestone, 21: Limestone, 22: Limestone “Liditas Formation”, 23: Greywacke Shale-Sandstone, 24: Andesite, 25: Black shale and carbon, 27: Red Sandstone, 32: Interbedded Sandstone, Limestone and silt, 49: Moraine, 52: Talus deposit, 53: Colluvium Deposit, 54: Alluvial Deposit, 55: Alluvial Fan. **a** and **b** are the case studies areas (modified from Rios-Araguez et al., 1987).

The climate in this area is characterised by a marked seasonality, classified as the Mediterranean mountain type with Atlantic and Continental influences (Creus and Gil, 2001). Part of the study area is covered by forests. However, forests have been replaced by cultivated fields that were abandoned at least from the middle of the 20th century (García-Ruiz and Lasanta, 1990).

In this area the anthropic print is significant: apart from the settlements of Portalet, Formigal and Sallent de Gallego, two dams, and the connection road to France, there is a wide ski-area. Due to the geological setting the area is affected by many landslides. Therefore, to acquire an updated landslides database is fundamental to support the territorial planning and infrastructure development. Various authors have studied the landslides and the geomorphology in the study area (García-Ruiz et al., 1995, 2004; Mulas and Fresno, 1995).

## 2.1 Geological and geomorphological setting

The study area is occupied by the magmatic and Paleozoic complex of the axial Pyrenees that is affected by the Hercinian folding phase. A geological map (Rios-Argues et al., 1987) is shown in Fig. 1. The centre of the valley is characterised by the outcrop of the Devonian Shale, whereas in the northern part this formation is overthrust by the Carboniferous Limestone formation. In the South-West

there is an outcrop of Permian sandstone, conglomerate and Carboniferous greywacke.

These materials are usually covered by Quaternary sediments: alluvial or alluvial fan deposits in the valley, and colluvial deposits on the slopes that present a significant thickness favoured by the weathering process of shale formations. The toe of the scarps are usually covered by talus or rockfall deposits. In the past, glacial action was very relevant especially in the upper part of the basin (SW area) with many glacial circle and morenic deposits. In some sites it is also possible to see the presence of rock glaciers that were probably active in the little Ice Age. In fact, the periglacial and slope processes are responsible for the shape of the landscape of the valley. The study area shows medium-low seismicity (Mulas et al., 2003), and is controlled by two tectonic lineaments following the NW-SE direction parallel to the valley and the SW-NE direction.

## 2.2 Landslides type and distribution

The type and distribution of landslides in the study area is controlled by the structural and geological setting, as well as by the glacial, the fluvial action and erosion. Massive rock outcrops (limestone, sandstone, conglomerate, and intrusive rocks) present an abrupt morphology with steep slopes (25–35°) and structural scarps. These lithologies are affected by rock fall or rock avalanche processes that favour the accumulation of rock deposits at the toe of the scarps.

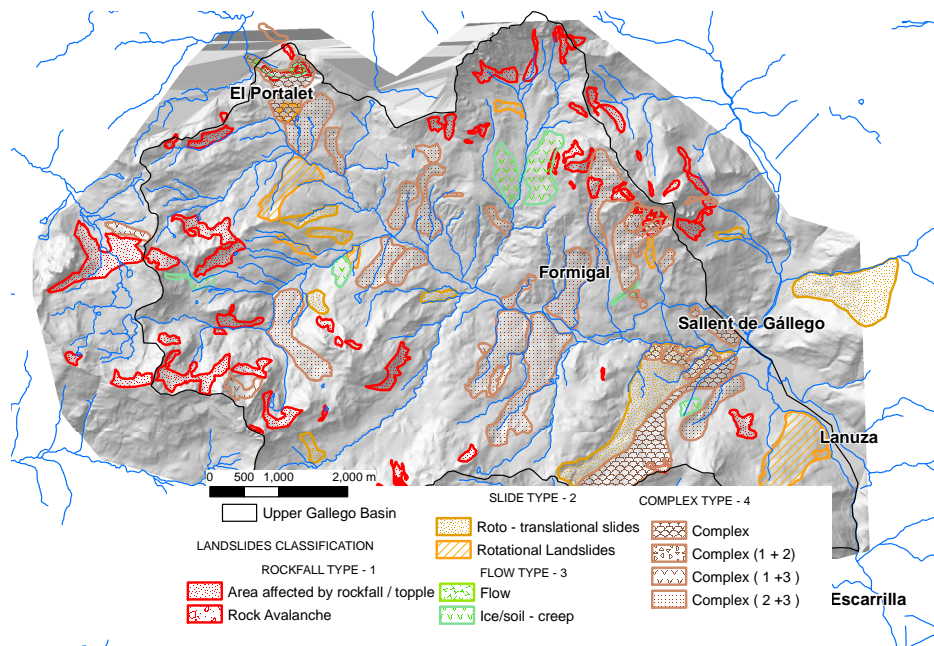


**Fig. 2.** The landslides inventory on Valle de Tena.

Shale formations occupy gentle slopes ( $15\text{--}20^\circ$ ), and present a considerable thickness of weathered rocks and colluvial deposits. These formations are usually affected by slow flow landslides, and soil/ice creep processes. Frequently these are shallow and active landslides, but deep-seated landslides can also be found. The mechanisms that control these landslides are complex and involve roto-translation with flow. In some cases, these landslides transport rock fall and rock avalanche deposits derived from the upper massive rock scarps. These landslides were triggered by the glacial retire and, nowadays, the whole body is in a relict state of activity. Nevertheless, local reactivation is frequently observing flow/slide movements triggered by the erosive action of River Gallego and the great seasonal variation of soil humidity in old landslide deposits. These reactivations affect infrastructures, mainly roads and ski area facilities. The presence of badlands and rill erosion can also be noticed in the area.

In order to analyse the performance of X-band data for landslide mapping, the pre-existing landslide inventories (García-Ruiz et al., 1995, 2004; Mulas and Fresno, 1995) have been revised and improved through the analysis of aerial photo, geological data and field survey. The landslide inventories map is shown in Fig. 2.

As a result the updated landslide inventory of the Upper Tena Valley consists of 103 landslides that cover about 28% of the total area. From the total amount 53% are paleo-landslides that affect the shale formations. These landslides are reactivated locally triggering flow and roto-translational slides. The areas affected by rock fall represent 47% of the total but they are usually of a smaller size. These type of

landslides are concentrated in the southwest and northern part of the study area where the steepest slopes and massive formations coincide.

### 3 PSI analysis : X-band SAR data and SPN processing

#### 4 SPN processing

The Stable Point Network (SPN) technique is a Persistent Scatterer Interferometry (PSI) technique developed by Arnaud et al. (2003) and Duro et al. (2005). In this work, a set of 14 TerraSAR-X Stripmap images of the Tena Valley was processed using the SPN technique. These data cover the period from May to October 2008, with time intervals between subsequent images of 11 or 22 days. The data were acquired with a descending orbit with an angle from north of  $80^\circ$  and the LOS (Line of Sight which is the line that goes from the radar antenna to the observed point on the ground surface) direction is  $278^\circ$  with an incidence angle of  $45^\circ$ . Considering a revisit time and the wavelength the maximum movement detectable between two measurements is about 0.75 cm in 11 days (25 cm/yr). The high acquisition frequency allowed to perform a PSI processing over a short temporal interval of only 6 months. This would be impossible using ERS or ENVISAT images, due to their larger temporal baselines of at least 35 days. The shorter period of analysis and the few images (11) used for processing can cause a higher error in the measuring of displacement. Usually the persistent scatterer processing requires of more than 15 images for an adequate performance (Wasowski et al., 2008).

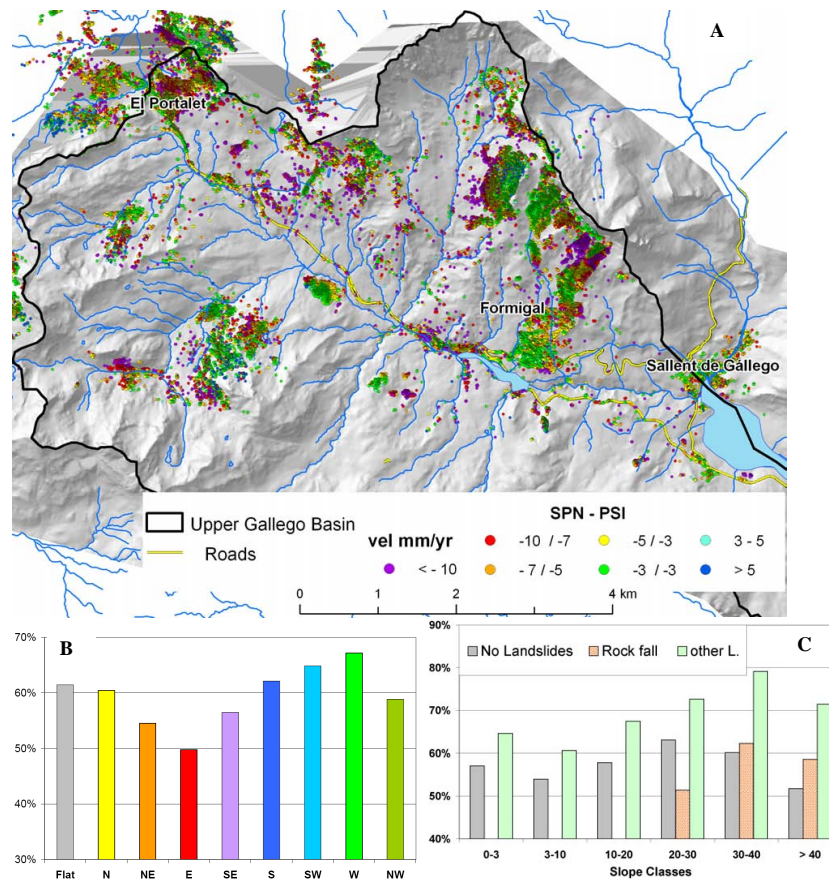


**Fig. 3.** (A) Radar displacement rate map; (B) distribution of displacement PS with respect to the slope dip direction (aspect); (C) distribution of displacement PS with respect to the slope inclination.

The SPN algorithm has been already used to process C-band data for mapping landslides in the study area (Herrera et al., 2009a, b) and also to process X-band data for monitoring a particular scenario: the Portalet landslide (Herrera et al., 2010). In these works a more detailed description of the SPN algorithm can be found.

#### 4.1 Spatial analysis of radar results

The processing of X-band SAR images with the SPN technique was permitted to detect over 35 000 Persistent Scatterers (PS) or measurement points ( $1000 \text{ PS}/\text{km}^2$ ) in the study area. In some areas a density greater than  $10\,000 \text{ PS}/\text{km}^2$  has been detected where rock fall and rock avalanche deposits are found. The retrieved radar deformation map is shown in Fig. 3a.

The analysis of the velocity of the detected PS show that, using a threshold of  $\pm 3 \text{ mm}/\text{yr}$ , the stable PS are 34% of total. The high percentage of PS (66%) with greater velocities (hereafter displacement PS) is due to the short monitoring period (only 6 months) that allows the detection of a high density of PS in areas affected by active superficial processes (debris flow, soil flux, erosion, etc.). In the case that the

monitoring period was longer, PS would be probably not detected in these kind of processes or at least in a lower amount.

If we analyse the percentage of displacement PS with respect to the slope dip direction (aspect) as well as with the slope angle, it is possible to identify two different effects:

1. The magnitude of the PS displacement rate depends on the slope dip direction (aspect). In this case study the slopes that are oriented to the west show a greater displacement rate than those oriented to the east (Fig. 3b). This is due to the acquisition geometry of the TerraSAR-X satellite, being  $278^\circ \text{ N}$  the descending orbit trajectory, and  $45^\circ$  the incidence angle. Note that displacement is measured in the Line of Sight (LOS) which is the line that goes from the radar antenna to the observed point on the ground surface. A detailed description of this topic can be found in Meisina et al. (2008) and Colesanti et al. (2006).
2. The slope angle influences the amount of detected displacement PS in landslides. In Fig. 3c, we observe that the greatest concentration of displacement PS on landslides coincides with greater slopes, except for

those greater than  $40^\circ$  that are rare. In fact, the greatest amount of displacement PS is found in slopes between  $30\text{--}40^\circ$  that usually correspond to the crown area of landslides. On the other hand, the percentage of displacement PS on rock fall type landslides seems not to be influenced by the slope. This is due to the relative stability of rock fall deposit that after the falls do not show further movements if they are not affected by other processes. The fall mechanism is too fast to be detected by this techniques.

## 5 A model to predict detectable areas using PSI techniques

One of the limitations of using PSI techniques to detect and monitor ground surface deformation is the uncertainty associated with the detection of measurement points (PS) (Colesanti and Wasowsky, 2004). Therefore, before using them it would be interesting to know if the presence of PS is possible. Colombo et al. (2006) presented a model to predict PS density discarding those areas susceptible to suffering layover and shadow effects and considering the land use. In this work, we propose an improved predictive model that takes into account the radar geometry, the slope angle, the slope dip orientation and the land use. Results are then compared and validated with X-band measurements.

### 5.1 The effect of the geometry

The satellite antenna emits electro waves that rebound in the ground surface and are received back with a time delay. The time delay is used to build the SAR image that is projected on radar coordinates (azimuth and slant range directions). The azimuth direction is defined by the satellite orbit trajectory, whereas the slant range direction is the line that goes from the radar antenna to the observed point on the ground surface, the so called Line of Sight (LOS) (Ferretti et al., 2001; Kropatsch and Strobl, 1990). Therefore, every ground surface target (ground range) is measured by the satellite sensor on radar coordinates (slant range). Depending upon the slope angle and the slope dip orientation, there are problems of geometry distortion (layover, foreshortening and shadow effects) that prevent the PS being detected (Colesanti and Wasowski, 2006).

Therefore, in order to estimate if PS can be detected or not in mountainous areas, we propose the *R-index equation* (Eq. 1) that is the ratio defined between the slant range and the ground range taking into account the acquisition geometry of the radar and the geometry of the ground surface (slope and aspect models derived from a DEM):

$$R = -\sin(\arctan(\tan S \cdot \sin A\alpha) - \theta) \quad (1)$$

$R$  = R-index,  $S$  = slope derived from DEM,  $A\alpha$  = aspect derived from DEM and correct with angle from north of the satellite track (i.e.  $-8^\circ$  for TerraSAR descending  $+188^\circ$  for ALOS ascending geometry),  $\theta$  = incident angle of LOS.

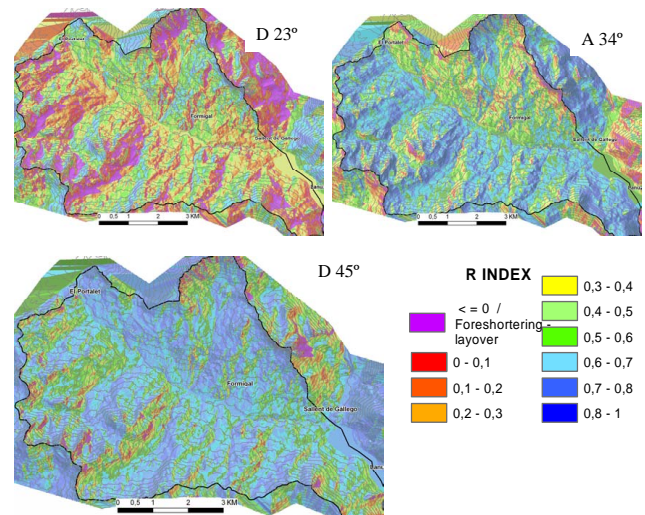


Fig. 4. R-index calculated for three different satellites.

The maximum value of the R-index is 1. This occurs when the slope is parallel to the LOS. This is the best geometry to detect PS in mountainous areas. On the other hand, the smaller the R-index, the more difficult it will be to detect PS.

The extreme case is when  $R$  tends to 0. This is the case of the foreshortening effect and no PS can be detected. The layover effect and the shadow effect occur when the R-index is negative and no PS can be detected.

In order to test this model, we have calculated the R-index for the Upper Valle de Tena study area, considering three different satellites with different LOS orientation (Fig. 6): (D  $23^\circ$ ) descending orbit with  $23^\circ$  incidence angle (like ERS and Envisat satellite); (A  $34^\circ$ ) ascending orbit with  $34^\circ$  of incidence angle (like ALOS PALSAR sensors); (D  $45^\circ$ ) descending orbit with  $45^\circ$  incidence angle (like TerraSAR-X sensor).

The results of the R-index calculation are shown in Fig. 4. It is interesting to observe that for the descending orbit, the greater the incidence angle, the greater the R-index i.e. the probability of detecting PS. On the other hand, if we compare ascending and descending orbits we see that the descending geometry is better for slopes oriented to the west, whereas the ascending geometry is better for those oriented to the east. Finally, in order to validate this model, the results were compared with the TerraSAR-X detected PS in the study area. The results of this comparison are shown in Table 1, where we can appreciate that the better the R-index is, the greater amount of detected PS and the greater the PS density.

### 5.2 The effect of the land use

The second major factor that influences the detection of PS is the presence of stable reflectors: buildings or other infrastructures (pylons, railways, etc.) rock and debris. The presence of stable reflectors in the ground surface can be

**Table 1.** R-index results against detected PS from TerraSAR-X dataset.

R-index classes	Pixel compression	N° (PS)	area (km <sup>2</sup> )	Density (PS/km <sup>2</sup> )
0 ≤=	layover/foreshortening – no PS	3	0.45	7
0–0.1	very high – bad slope	4	0.23	17
0.1–0.2	high – bad slope	6	0.59	10
0.2–0.3	high – bad slope	15	1.33	11
0.3–0.4	medium - high	78	2,36	33
0.4–0.5	medium	336	3.80	89
0.5–0.6	medium	1641	6.24	263
0.6–0.7	medium-low – quite good slope	5325	8.23	647
0.7–0.8	low good slope	10 039	7.54	1332
>0.8	very low good slope	17 936	7.46	2404
<i>0.707 single value</i>	<i>flat area case</i>	600	1.25	481
Total area		35 983	39.48	911

**Table 2.** PS index values based on the land use classifications derived from CORINE (LU index).

LU index	0	10	20	30	80	90	100
Land use	Water	Forest	Grass	Sparse vegetation	Rock	Debris	Urban area

estimated from the land use map. Therefore, the integration of land use data in the proposed geometrical model can improve the prediction of those areas where PS maybe detected.

Reaching this point, it is important to point out that the quality of the estimation will depend on the quality of the land use data. In this case, we have used CORINE land use information. For this purpose we have assigned a unique land use index, “LU index” for each land use class, which varies from 0 (no PS can be detected) to 100.

The “LU index” values (Table 2, Fig. 7b) were assigned based on previous PS-land use comparisons (Colombo et al., 2006). Since we have observed that both the “R-index” and the “LU index” have a similar importance, we propose the corrected R-index or “RC index” following Eq. (2). The “RC index” varies from 0 to 100, where 0 represents those areas where PS can not be detected and 100 represents those areas with a high density of PS. Note that whenever either the “R-index” or the “LU index” are zero, we assign zero to the RC index.

$$\text{RC index} = (\text{R-index} * 100 + \text{LU index}) / 2; \quad (2)$$

The results from the RC index are shown in Fig. 5 and in Table 3. In this case, we can observe how the land use of the study area is a greater limit for the detection of PS than the geometrical aspects. Note that only 26% of the study area is covered by land use with a LU index greater than 50

(average susceptibility to detect PS), whereas in the case of the R-index, 75% of the study area show values greater than 50. If we analyse the results of the RC index summarised in Table 3, we can observe that there is a good agreement between RC index predictions and the PS density detected from the TerraSAR-X data analysis. Note that the PS density is low when the RC index is smaller than 50, and when the RC index is greater than 80 the highest concentration of PS is found.

## 6 Landslides analysis based on X-band data

### 6.1 Comparison of the radar data with the landslide inventory

The PSI techniques provide important information about landslides (Wasowski et al., 2008). They can be used to detect landslides that are not previously known (Meisina et al., 2008) or to re-define the geometry of existing landslides (Fernandez et al., 2009); and they can also be used to monitor landslides but not in real-time (Catani et al., 2006). In order to fully exploit PSI techniques capabilities, it is necessary to analyse the distribution of detected PS within the different types of landslides. When comparing the PS dataset with the landslide inventory in the study area, we have observed that only 54 landslides (53% of total) show 1 or more PS. Reaching this point, it is fundamental to define

**Table 3.** RC index compared with PS density.

RC index	Area (km <sup>2</sup> )	Num (PS)	Area (%)	PS (%)	Density (PS/km <sup>2</sup> )
0	0.420	2	1.3%	0.0%	5
0–10	–	–	–	–	–
10–20	0.091	1	0.3%	0.0%	11
20–30	0.814	19	2.5%	0.1%	23
30–40	4.437	314	13.8%	0.9%	71
40–50	10.066	2833	31.4%	8.4%	281
50–60	9.161	9784	28.6%	28.9%	1068
60–70	2.513	2801	7.8%	8.3%	1114
70–80	1.683	1694	5.3%	5.0%	1006
80–90	1.577	6331	4.9%	18.7%	4015
90–100	1.283	10 054	4.0%	29.7%	7837
Total	32	33 833	100.0%	100.0%	1056

the parameters that need to be taken into account to decide if detected PS are indicative or not of landslide displacement. We consider the following parameters:

Number and density of PS: at least 3 PS and a density up to 100 PSI/km<sup>2</sup> within the landslide.

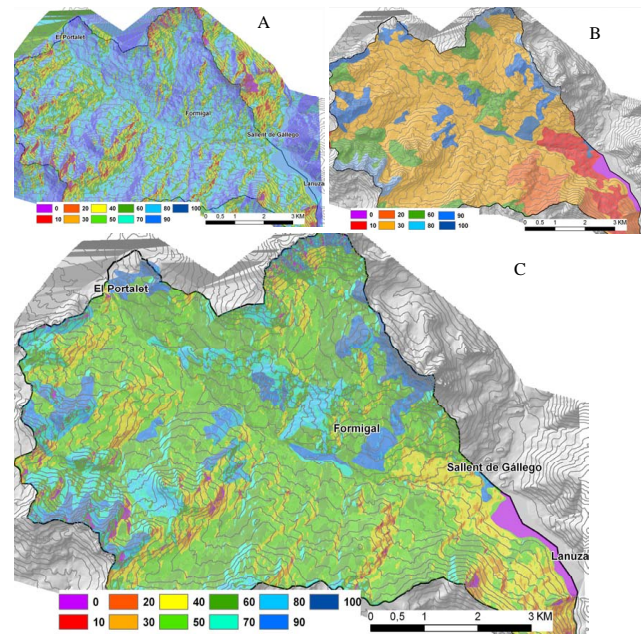
Locations and typology of PS: in some situations the PS data are concentrated in a little area that may be of interest. This is the case of PS close to buildings or to other infrastructures, such as roads.

Landslides typology: only slow landslides (<100 mm/yr) can be detected and monitored. For the other type of landslides (i.e. rock fall) the PS data maybe in some cases considered as precursor of rupture (Herrera et al., 2010).

After taking into account this aspects in the study area the landslides suitable for PS analysis are only 22 (21% of total and 54% of the total if we consider only the slow type landslides).

## 6.2 The anomalous areas: a method to detect possible “new landslides”

When a database is composed of a large number of PS over a wide area it is important to identify displacement areas where the PS can give significant information about the dynamics of the existing geological processes (landslides, subsidence, etc.). These “anomalous areas” are characterised by a high PS density that measure displacements. A procedure to detect anomalous areas for the regional interpretation of C-band data was proposed by Meisina et al. (2008) and using the hot spot analysis by Lu et al. (2009). This kind of procedure has been proved to be very useful to detect slow landslides and even to detect areas affected by the unknown.

**Fig. 5.** A R-index\*100, B Landuse Index (LU), C RC index.

In this test site the exploitation of X-band data provides a great density of PS. Therefore, in order to detect anomalous areas we have performed an IDW (Inverse Distance Weighted) interpolation of the displacement velocity values of those areas with more than 1000 PSI/km<sup>2</sup> and then we have selected those areas greater than 1000 m<sup>2</sup> with an average displacement rate greater than 5 mm/yr. In Fig. 6, we see that there is a good correlation between the estimated anomalous areas and mapped landslides. Moreover, these approaches have permitted us to identify 4 new landslides and to redefine the boundaries of 8 other landslides. It is important to underline that not all of the anomalous areas correspond to landslides: in some cases the movement can be explained with the settlement of new buildings or other processes; in other cases the movement is not easy to understand and further investigations are required.

## 7 Case of studies

In this section, we present two case studies where the performance the PSI processing of X-band data can be evaluated for landslide mapping and monitoring. In the first case, we show how a great density of PS data permit the defining of the surface dynamics of a landslide where no other information is available (Fernandez et al., 2009). In the second case, we show a landslide where the PS data are insufficient to characterise the mass movement dynamics, but it is useful to detect the displacements affecting a road located at the toe of the landslide.

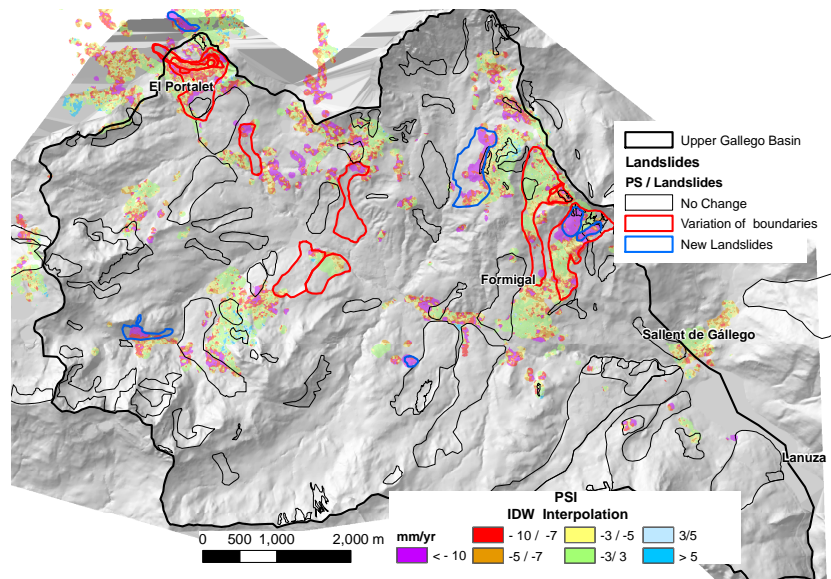


**Fig. 6.** IDW interpolation of PS data and landslides. In blue the “landslides detected with PSI, in red the landslides in which PSI data is useful to redefine limits.

### 7.1 The Formigal landslide

The Formigal area is a very good example of a landslide where the PSI technique provides a great PS density but little information is available: the ortho-images, the regional geological and geomorphological map, and some pictures taken on a field trip.

The geological setting is defined on the top by the limestone formation (Foratata Peak) where rock fall and rock avalanche processes are found. The associated rock deposits are found spread from the upper to the lower part of the slope where highly weathered and altered shale formations are found. The area close to Formigal village is affected by three large deep seated paleo-landslides (1-2-3 in Fig. 7a) of the complex type. As it has been previously described these landslides were triggered by glacial retire. Now the whole body of these landslides can be considered inactive, even though within their area of influence slow flows of the weathering shale formations are present. As seen in Fig. 9, the dynamics of these processes have been detected and monitored with great detail with the SPN analysis of X-band SAR data. A very high PS density has been detected especially on the rock deposits located at the toe of the scarps ( $15\,000\text{ PS/km}^2$ ), as well as in the urban area of Formigal ( $7\,000\text{ PS/km}^2$ ). In the upper part at the toe of the limestone cliff it is possible to identify two areas with strong movement separated by a stable area. From the PS data analysis it is possible to identify different processes that are confirmed by the evidence of aerial photo and field survey (Fig. 9a, b). Therefore, the PS data allow us to recognize three main areas in landslide 1:

- The area 1A in Fig. 7 corresponds to a large slow flow landslide with a convex profile that in the upper part

presents a strong movement from the point of view of radar measurements (up to  $10\text{ mm/yr}$ ). In this case the detected PS corresponds to the rock fall blocks from the upper limestone scarps. The landslide is extended downhill towards the village of Formigal where it joins the toe of landslide 2. In this area detected movements show a stable behaviour.

- Area 1S in Fig. 7 is covered by talus and rock avalanche deposits. This area presents a more regular slope and the vegetation coverage is evident of a lack of displacement that is confirmed by the detected PS. It is interesting to observe that this stable area presents clearly defined boundaries with respect to the neighbouring unstable areas.
- Area 1B in Fig. 7 is a rock avalanche deposit that is placed in the concave part of the slope. The size of the blocks is from metres to decametres. Now the movements are mainly related to slow flow processes that affect the underlying soil and the weathered shale. In the middle part of slope Area 1B joins Area 1A. Therefore, both areas can be considered as part of a single complex landslide with a prevalent flow mechanism. Note that the high density of PS detected in the upper part of the slope allows for accurate delimiting of the areas with movement from the stable areas. This is something that cannot be done with other traditional remote-sensing techniques.

The landslide 2 is placed in the slope north from Formigal and in the upper part it is separated by a small ridge from landslide 1. In this landslide the PS data do not show areas with strong movements except for the upper

eastern part (2A in Fig. 7) and the scarps located at 1800 m a.s.l. (2B in Fig. 7). The toe of this landslide 2 affects the upper part of Formigal village where slow to moderate displacements have been detected. These displacements correspond to the settlement of new buildings and infrastructures that have been identified through the comparison of two aerial photos from different periods, 2000 and 2006 (red polygon in Fig. 7). This example illustrates the importance of checking the PS data with other available information in order to avoid misinterpretations of the SAR data.

Finally the landslide 3, which is placed at the west from Formigal in the middle part of the slope, presents very few PS that do not show significant displacements.

## 7.2 Road close to Formigal

This case study shows that even though the X-band data could not detect displacement on the targeted landslide, it was useful to detect and monitor the effects of the landslide on the road.

This complex landslide affects the shale formations and it is placed on the right side of the Upper Tena Valley. The lowest part has affected the road repeatedly since the 1970s (Bixel et al., 1985; IGME, 1988) due to many local reactivations triggered by the erosion of Gállego River.

Due to the bad orientation of the slope and to the land use (forests cover) of this landslide, not many PS were detected from the descending orbit of TerraSAR-X dataset. As a matter of fact, the detected PS are concentrated at the toe of the landslide coinciding with the road infrastructure and do not permit the measurement of the whole dynamic of the landslide. Nevertheless, the detection of displacement PS along the road infrastructure is indicative of the activity of the lowest part of the landslide and can be correlated with local damages. A field survey in summer 2009 showed that the section of the road, which is within the lowest part of the landslide (Fig. 8a), presents many damages like tension cracks, bumping and deformations that fit well with the PS data (Fig. 8b and c).

The detected PS correlate well with the small slide scarps (the polygon D show in the Fig. 8a and d). This example shows that the X-band dataset provides displacement information of very small unstable areas.

## 8 Conclusions

The technical and economical evaluation of applying radar remote-sensing techniques to landslides mapping requires us to know beforehand the advantages and disadvantages of using these techniques in the area of interest. Overall, Persistent Scatterer Interferometry permits the detection and monitoring precisely (with a metric spatial precision and millimetric velocity error) slow (<10 cm/yr) landslides

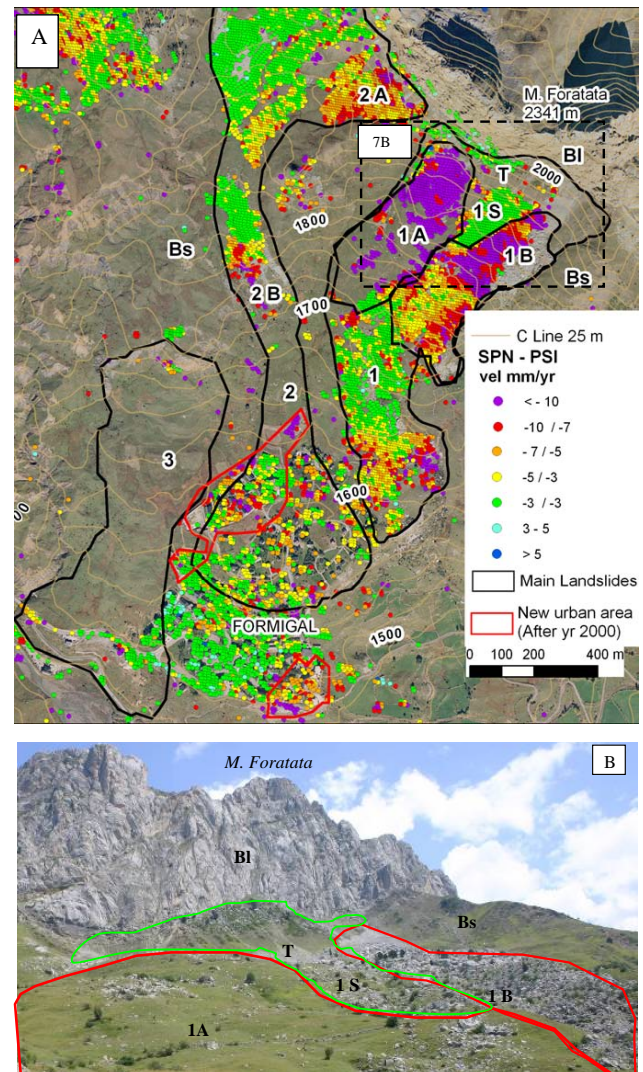


**Fig. 7.** **A** Displacement rate measured in Formigal landslide. **B** Complex landslides with rock fall blocks; 1S: stable area covered by talus (T) and rock fall deposit; 1B: rock avalanche deposit over a slow flow; BI: Bedrock Limestone; Bs: bedrock shale.

depending on several factors: (1) the temporal sampling and the geometry of the acquisition satellite; (2) the geometry of the area of interest; and (3) the land use. The evaluation of these factors through a spatial analysis allows the foresight of the distribution and density of PS that may be detected. Therefore, this kind of analysis may be useful to select the most suited satellite sensor for the area of interest as well as the best radar processing strategy. In this work, we propose a model that predicts the PS presence based on the satellite radar geometry, the slope orientation, the slope angle and the land use. The comparison of predicted PS distribution with detected PS from the X-band dataset has validated the proposed model. However, some errors may exist depending upon the quality of input data (DEM and land use).

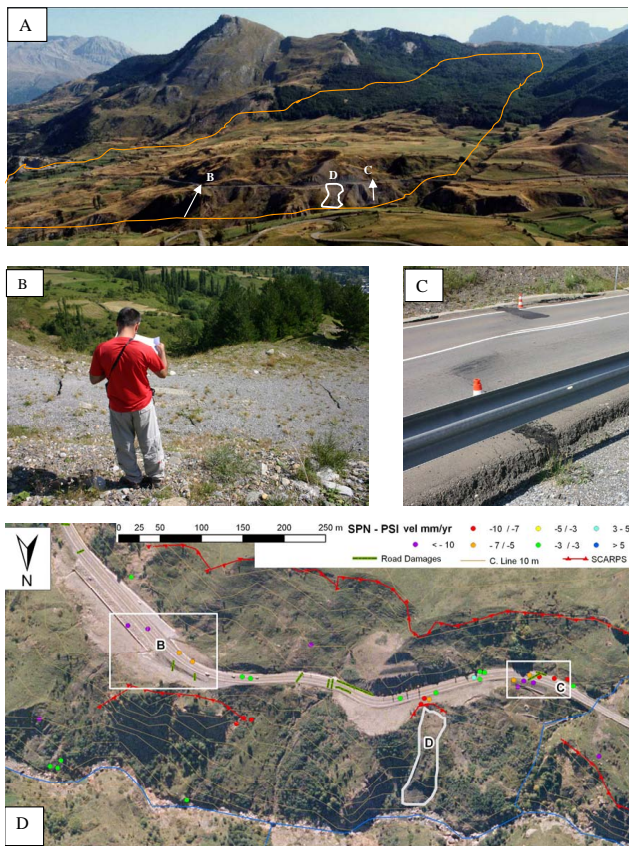


**Fig. 8.** A View of the landslides in 1989 (IGME), B and C road damages, tension cracks and small slide scarps in the summer 2009, D displacement PS close to small landslide crown.

In the whole study area the average density of detected PS is  $1000 \text{ PS}/\text{km}^2$ , even though it depends very much on the geometry and the land use. Note that in favourable areas rock fall or rock avalanche deposits can reach over  $10\,000 \text{ PS}/\text{km}^2$ . Attending to the retrieved high PS density and the displacement rate values we have performed an interpolation of PS data in order to select those areas where movement is significant, the “anomalous areas”. These areas coincide well with mapped landslides, but they have also been useful to detect new landslides and to modify the boundaries of pre-existing ones. For this purpose it has been necessary to perform a geological interpretation with traditional methods in order to determinate the cause of movement. Overall, the landslide analysis based on X-band data has allowed to: (1) improve the existing landslide database (three new landslides were added to the database and the boundaries of another 4 were re-drawn); and (2) to monitor 50% of the inventoried slow landslides. In the next future a more detailed geomorphological mapping of the study area will permit to improve the exploitation of this results.

Finally, the presented case studies have demonstrated that the exploitation of X-band data maybe useful to: (1) define with a great spatial and temporal resolution the different surface dynamics within a landslide where little information is available; and (2) to detect local displacements that may affect infrastructures. Therefore, the integration of this kind of analysis can be a valuable tool for territorial management and infrastructures surveillance strategies.

*Acknowledgements.* This work has been partially funded by the project SPAINSLIDES element of the of the TerraFirma Global Monitoring for Environment and Security program from ESA, by the project DO-SMS (SUDOE INTERREG IV B) by the Spanish Geological and Mining Institute (IGME), and by the University of Pavia. The authors acknowledge the ERASMUS mobility program for PhD students, that permitted Davide Notti to perform a research internship resulting in the elaboration of this work. The digital elevation model and aerial photographs used in this work have been provided by the cartographical service of the government of Aragón.

Edited by: R. Lasaponara

Reviewed by: two anonymous referees

## References

- Arnaud, A., Adam, N., Hanssen, R., Inglada, J., Duro, J., Closa, J., and Eineder, M.: ASAR ERS interferometric phase continuity, IGARSS, Toulouse, France, CDROM, 21–25 July 2003.
- Berardin, P., Fornaro, G., Lanari, R., and Sansost, E.: A new algorithm for surface deformation monitoring based on small baseline differential Interferograms, *IEEE T. Geosci. Remote*, 40(11), 2375–2383, 2002.
- Bixel, F., Muller, J., and Roger, P.: Carte géologique du Pic du Midi d’Oussau et haut bassin du rio Gállego, 1:25.000, Institut de Géodynamique, Université de Bordeaux, Bordeaux, 54 pp., 1985.
- Cascini, L., Fornaro, G., and Peduto, D.: Analysis at medium scale of low-resolution DInSAR data in slow-moving landslide-affected areas, *ISPRS Journal of Photogrammetry and Remote Sensing*, 64(6), 598–611, November 2009.
- Catani, F., Colombo, D., Farina, P., Fumagalli, A., Kukavicic, M., Marks, F., Menduni, G., and Moretti, S.: Utilizzo di dati telerilevati nella mappatura e nel monitoraggio dei fenomeni franosi e nell’analisi della suscettibilità da frana, *Giornale di Geologia Applicata*, 3, 173–180, doi:10.1474/GGA.2006-03-0-23.0116, 2006 (in Italian).
- Colesanti, C. and Wasowski, J.: Investigating landslides with spaceborne Synthetic Aperture Radar (SAR) interferometry, *Eng. Geol.*, 88(3–4), 173–199. doi:10.1016/j.eng geo., 2006.
- Colesanti, C. and Wasowski, J.: Satellite SAR interferometry for wide-area slope hazard detection and site-specific monitoring of slow landslides, *Proc. Ninth Int. Symp. Landslides, Rio de Janeiro, Brazil*, 795–802, 2004.
- Colombo, A., Mallen, L., Pispico, R., Giannico, C., Bianchi, M., and Savio, G.: Mappatura regionale delle aree monitorabili mediante l’uso della tecnica PS, In *Proceedings of 10° National Conference ASITA, Bolzano, ISBN/ISSN:88-900943-0-3-2006, 14–17 November 2006* (in Italian).

- Creus, J. and Gil, M.: Clima, in: *Estudio del Medio Físico y de sus Riesgos Naturales en un Sector del Pirineo Central*, Instituto Geológico y Minero de España, 39–41, 2001 (in Spanish).
- Crosetto, M., Crippa, B., Biescas, E., Monserrat, O., Agudo, M., and Fernandez, P.: Land deformation monitoring using SAR interferometry: state-of-the-art, *Photogramm. Fernerkun.*, 6, 497–510, 2005.
- Farina, P., Colombo, D., Fumagalli, A., Marks, F., and Moretti, S.: Permanent Scatterers for landslide investigations: outcomes from ESA-SLAM project, *Eng. Geol.*, 88, 200–217, 2006.
- Ferretti, A., Prati, C., and Rocca, F.: Permanent scatterers in SAR interferometry, *IEEE T. Geosci. Remote*, 39(1), 8–20, 2001.
- Fernández, P., Irigaray, C., Jiménez, J., El Hamdouni, R., Crosetto, M., Monserrat, O., and Chacón, J.: First delimitation of areas affected by ground deformations in the Guadalfeo River Valley and Granada metropolitan area (Spain) using the DInSAR technique, *Eng. Geol.*, 105, 84–101, doi:10.1016/j.enggeo.2008.12.005, 2009.
- García-Ruiz, J. M., Chueca, J., and Julián, A.: Los movimientos en masa del Alto Gállego, in: *Geografía Física de Aragón*, edited by: Peña, J. L., Longares, L. A., Sánchez, M., Aspectos Generales y Temáticos, 142–152 pp., 2004 (in Spanish).
- García-Ruiz, J. M., Martí-Bono, C., and Gómez-Villar, A.: Mapa Geomorfológico: Sallent (Huesca), in: *Estudio del Medio Físico y de sus Riesgos Naturales en un Sector del Pirineo Central*, Instituto Geológico y Minero de España, Report, 35 pp., 1995 (in Spanish).
- García-Ruiz, J. M. and Lasanta, T.: Land use changes in the Spanish Pyrenees, *Mt. Res. Dev.*, 10, 267–279, 1990.
- IGME: Estudio de riesgos geológicos inducidos por varios deslizamientos que afectan a la carretera C-136 (entre el Km 91.600 y 92,500; cerca de la estación de esquí de Formigal), Instituto Geológico y Minero de España, Informe inédito, 77 pp., 1988 (in Spanish).
- Herrera, G., Davalillo, J. C., Mulas, J., Cooksley, G., Monserrat, O., and Pancioli, V.: Mapping and monitoring geomorphological processes in mountainous areas using PSI data: Central Pyrenees case study, *Nat. Hazards Earth Syst. Sci.*, 9, 1587–1598, doi:10.5194/nhess-9-1587-2009, 2009a.
- Herrera, G., Fernández-Merodo, J. A., Mulas, J., Pastor, M., Luzi, G., and Monserrat, O.: Use of ground based sar data in landslide forecasting models: the Portalet case study, *Eng. Geol.*, 105(3–4), 220–230, 2009b.
- Herrera, G., Notti, D., García-Davalillo, J. C., Mora, O., Cooksley, G., Sánchez, M., Arnaud, A., and Crosetto, M.: Landslides analysis with C- and X-band satellite SAR data: the Portalet landslide area, *Landslides*, in press, doi:10.1007/s10346-010-0239-3, 2010.
- Kropatsch, W. G. and Strobl, D.: The generation of SAR Layover and shadow amps from digital elevation models, *IEEE T. Geosci. Remote*, 28(1), 98–107, 1990.
- Lu, P., Catani, F., Casagli, N., and Tofani, V.: Hotspot analysis of Permanent Scatterers (PS) for slow-moving landslides, in: *Proceedings of Landslide Processes: from geomorphological mapping to dynamic modelling*, Strasbourg, France, 57 pp., 2009.
- Meisina, C., Zucca, F., Notti, D., Colombo, A., Cucchi, A., Savio, G., Giannico, C., and Bianchi, M.: Geological interpretation of PSInSAR data at regional scale, *Sensors*, 11, 7469–7492, 2008.
- Meisina, C., Zucca, F., and Notti, D.: Regional interpretation of PSInSAR(TM) data for landslide investigations, In *Proceedings of EGU 2010 General Assembly*, Vienna, 3–7 May 2010.
- Meisina, C., Zucca, F., Fossati, D., Ceriani, M., and Allievi, J.: Ground deformation monitoring by using the Permanent Scatterers Technique: The example of the Oltrepo Pavese (Lombardia, Italy), *Eng. Geol.*, 88, 240–259, 2006.
- Mora, O., Mallorquí, J. J., and Broquetas, A.: Linear and nonlinear terrain deformation maps from a reduced set of interferometric SAR images, *IEEE T. Geosci. Remote*, 41(10), 2243–2253, 2003.
- Mulas de la Peña, J. and Fresno-López, F.: *Estudio Geotécnico y de Riesgos Naturales. Estudio del Medio Físico y de sus Riesgos Naturales en un Sector del Pirineo Central*, Instituto Geológico y Minero de España, Report, 216 pp., 1995 (in Spanish).
- Notti, D., Meisina, C., Zucca, F., Colombo, A., Cucchi, Savio, G., Giannico, C., and Bianchi, M.: PS interferometry-based studies of landslides at regional scale In *Proceedings of The First World Landslide Forum United Nations University*, Tokyo, Japan, 439–442, 2008.
- Pancioli, V., Raetzo, H., Campolmi, T., and Casagli, N.: TerraFirma Landslide Services for Europe based on Space-borne InSAR Data, in: *Proceedings of The First World Landslide Forum United Nations University*, Tokyo, Japan, 81–84, 2008.
- Pepe, A., Sansosti, E., Berardino, P. and Lanari, R.: On the Generation of ERS/ENVISAT DInSAR Time-Series via the SBAS technique, *IEEE T. Geosci. Remote S.*, 2, 265–269, 2005.
- Righini, G., Pancioli, V., and Casagli, N.: Updating landslide inventory maps using Persistent Scatterers Interferometry (PSI) in the Biferno River Basin (Central Italy), in: *Proceedings of EGU 2010 General Assembly*, Vienna, 3–7 May 2010.
- Rios-Argues, L. M., Galera-Fernandez, J. M., and Baretino-Fraile, D.: Mapa Geologica de España escala 1:50'000 F. 145 – Sallent de Gallego, Instituto Geológico Y Minero de España , 1987 (in Spanish).
- Strozzi, T., Delaloye, R., Käab, A., Ambrosi, C., Perruchoud, E., and Wegmüller, U.: Combined observations of rock mass movements using satellite SAR interferometry, differential GPS, airborne digital photogrammetry, and airborne photography interpretation, *J. Geophys. Res.*, 115, F01014, doi:10.1029/2009JF001311.
- Wasowski, J., Bovenga, F., Florio, N., and Gigante, G.: PSInSAR for the investigating of unstable slopes and landslides, in: *Proceedings of the 1st World Landslide Forum*, Tokyo, Japan, 653–655, 2008.